HHS Public Access

Author manuscript

Bioalgorithms Medsyst. Author manuscript; available in PMC 2024 July 30.

Published in final edited form as:

Bioalgorithms Medsyst. 2023 ; 19(1): 9–16. doi:10.5604/01.3001.0054.1817.

Application of quantum entanglement induced polarization for dual-positron and prompt gamma imaging

Gregory Romanchek[1,A,B,C,D,E,F], **Greyson Shoop**[2,A,B], **Shiva Abbaszadeh**[2,A,E,G]

[1]Department of Nuclear, Plasma, and Radiological Engineering, University of Illinois Urbana-Champaign, Urbana, USA

[2]Department of Electrical and Computer Engineering, University of California at Santa Cruz, Santa Cruz, USA

Abstract

The intrinsic resolution of Positron Emission Tomography (PET) imaging is bound by positron range effects, wherein the radioactive decay of the imaging tracer occurs at a disjoint location from positron annihilation. Compounding this issue are the variable ranges positrons achieve, depending on tracer species (the energy they are emitted with) and the medium they travel in (bone vs soft tissue, for example) – causing the range to span more than an order of magnitude across various study scenarios (~0.19 mm to ~6.4 mm). Radioisotopes, such as Zr-89, exhibit dual emissions of positron and prompt gammas, offering an opportunity for accurate tracer positioning as prompt gammas originate from the tracer location. These multi-emission radiotracers have historically suffered from increased noise corresponding to the third gamma interfering in annihilation gamma coincidence pairing. Recent advancements, however, have brought to light the unique property of annihilation gammas having scattering kinematics distinct from random gamma pairs. These properties are born from the singular quantum entanglement state available to the gamma pair following para-positronium decay which prescribes linearly orthogonal polarization. Such coherent polarization is not shared by prompt gamma emissions, offering an opportunity for their discrimination. We present an investigation into this technique, comparing the distribution of relevant scattering kinematics of entangled annihilation gammas and corresponding prompt gammas via a Monte Carlo simulation.

CORRESPONDING AUTHOR: Gregory Romanchek; Department of Nuclear, Plasma, and Radiological Engineering, University of Illinois Urbana-Champaign, Urbana, USA; 104 S Wright St, Urbana, IL 61801, USA; romanch2@illinois.edu.

AUTHORS' CONTRIBUTION:

A – Study Design
B – Data Collection
C – Statistical Analysis
D – Data Interpretation
E – Manuscript Preparation
F – Literature Search
G – Funds Collection

Keywords

PET Imaging; Prompt Gammas; Quantum Entanglement; Noise Reduction; Background Reduction

INTRODUCTION

The physics of electron-positron annihilation dictates that the resulting 511 keV annihilation gamma pair is generated in an entangled state. While we leave the description of this phenomena to the literature [1–3], the consequence of interest to this work is the entangled gammas' joint double differential cross section (DDCS) which cannot be described in the absence of quantum entanglement (QE). Such entangled gammas are exactly detectable in positron emission tomography (PET). PET imaging requires the detection of both annihilation gammas in order to draw a line-of-response (LOR) between their detection positions, with the assumption that the positron emitting isotope (the tracer) lays along this line. However, if either gamma scatters or of the gammas are incorrectly paired, the resulting LOR will contaminate the LOR data set – these are commonly referred to as scatters and randoms. Moreover, the tracer does not necessarily fall on the LOR; instead, the annihilation event, which may be millimetres from the original emission location, does.

Multi-emission isotopes, such as ^{89}Zr, produce prompt gammas in addition to positrons. Typically, non-annihilation gammas would only increase the random rate by complicating coincidence pairing. However, an advantage of prompt gammas is their colocation with the tracer position. These prompt gammas may therefore be used to correct for positron range effects with the appropriate technique. In terms of QE, the prompt gamma scatters independently of the annihilation gammas' entanglement. This raises the question of whether the unique scattering kinematics of entangled annihilation photons can be used to distinguish them from prompt gammas to combat the elevated noise they introduce.

The Klein-Nishina formula describes the differential cross section of photons undergoing scatter events and is given by:

$$\frac{d\sigma}{d\Omega} = \frac{r_e^2}{4}\left(\frac{E'}{E}\right)^2\left(\frac{E'}{E} + \frac{E}{E'} - \sin^2(\theta)\right), \tag{1}$$

where σ is the scattering cross section, Ω is the solid angle, r_e is the classical electron radius, E and E' are the initial and final gamma energies, respectively, and θ is the polar scattering angle. Eq. 1 only describes unpolarized photons and is thus an incomplete description for the polarized annihilation photons. This formula can be expanded to account for polarization as:

$$\frac{d\sigma}{d\Omega} = \frac{r_e^2}{4}\left(\frac{E'}{E}\right)^2\left(\frac{E'}{E} + \frac{E}{E'} - 2\sin^2(\theta)\cos^2(\phi)\right), \tag{2}$$

where ϕ is the azimuthal scattering angle. In Eqs. 1 and 2, we can note that the energy ratio can be substituted with

$$\frac{E'}{E} = \frac{1}{1 + \frac{E}{m_e c^2}(1 - \cos(\theta))} \tag{3}$$

where m_e is the rest mass of an electron and c is the speed of light. In PET, we can assume that the initial gamma energy is 511 keV, such that the $E/(m_e c^2)$ term simplifies to 1. For the two annihilation photons, one may assert that the DDCS could be written as:

$$\frac{d^2\sigma_{double}}{d\Omega_1 d\Omega_2} = \left(\frac{d\sigma_1}{d\Omega_1}\right)\left(\frac{d\sigma_2}{d\Omega_2}\right) \tag{4}$$

with the assumption that scattering in independent. However, this formulation does not account for their entanglement. Instead, we must use [4]:

$$\frac{d^2\sigma_{double}}{d\Omega_1 d\Omega_2} = \frac{r_e^4}{16}[K_a(\theta_1, \theta_2) - K_b(\theta_1, \theta_2) \cdot \cos(2\Delta\phi)], \tag{5}$$

where K_a and K_b are a collection of terms dependent on θ_1 and θ_2 and are described in the supplement of reference [4]. We note that the only presence of ϕ_1 or ϕ_2 is in the $\Delta\phi = \phi_1 - \phi_2$ term. The scattering potential is then maximized over azimuthal scattering for $\Delta\phi = \pm 90°$ and minimized for $\Delta\phi = 0°, \pm 180°$. Such a case is not true for the DDCS in Eq. 4 when using Eq. 1 for the individual differential cross sections. In the case of using Eq. 2, the polarized case, this same optimization is only true for orthogonally polarized photons, which have an equivalent rate of occurrence as any other polarization state given two randomly linearly polarized photons. And in this case, the difference between the maximum and minimum values is greater for the entangled case – this ratio is referred to as the enhancement factor and is the target of potential filtering techniques.

While the DDCS of two entangled gammas is described by Eq. 5, the DDCS of two non-entangled gammas (randoms and, disputably [5], scatters) is described by the substation of Eq. 2 into Eq. 4. These describe fundamentally distinct scattering kinematics, which may be leveraged for discriminating between the two scenarios. To do so, double Compton scatter events (DCSc) need to be observed, wherein each detected gamma undergoes an initial Compton scatter followed by a photoelectric absorption, depicted in Fig. 1. The scattering vectors can then be used to extract the scattering angles, which may be subsequently used to potentially classify the DCSc as associated with a true coincidence or a false coincidence. The simplest method would be to use a $\Delta\phi$ of about 90°, which favours true coincidences. In this report, we investigate this strategy through analytic and simulation methods to investigate its feasibility or to recommend alternative strategies.

MATERIAL AND METHODS

Analytic Methods

The single and double differential cross sections physics outlined in the Introduction are used to create a set of occurrence fields as a function of polar and azimuthal scattering angles. These fields are normalized to the minimum differential scattering cross section, such that 1) the minimum is unity, and 2) the normalized value represents how many times more it is likely to occur than that minimum. With these, we showcase the relative occurrence rate of ϕ scattering between varied polarization and entanglement states of annihilation gamma pairs.

$\Delta\phi$ Filtering

Using a simple $\Delta\phi$ threshold to filter DCSc on an event-by-event basis is implausible because non-entangled gamma pairs (namely, randoms and scatters) may still coincidentally exhibit orthogonal polarization. Thus, there will always be a non-zero False Positive rate. While this scenario theoretically happens with less frequency for non-entangled than entangled pairs and should then guarantee a >50% discrimination success rate (a low bar in and of itself for a classification task), this count is on a unitary basis – or in the case where the true rate equals the false rate. When accounting for the comparative noise and true coincidence rates, we may encounter discouraging results. Here, we use previously characterised true and noise coincidence count rates for our 2-Panel system to scale the analytic expectations and showcase the consequences of $\Delta\phi$ filtering with reality in mind.

GATE Simulations

GATE, a Geant4-based physics toolkit, serves as the dominant Monte Carlo physics simulator in the medical imaging research community [6]. We activate in GATE the Watt et al's QE-expansion of the Geant4 positron annihilation and Livermore polarized Compton models, which includes the entanglement-based annihilation gamma cross sections as defined by Eq. 5 [4, 7, 8]. With this physics toolkit, we conduct a series of GATE simulations using the novel UCSC 2-Panel PET scanner, currently under construction in our lab, to illustrate the impact of scattering physics (Fig. 2. [9, 10]).

The 2-Panel scanner constitutes two sets of one-hundred fifty $40 \times 5 \times 40$ mm^3 CZT crystals placed in a 5×30 array. These 15×20 cm^2 detector-face panels are separated by an adjustable 20 cm. While the decay and particle interaction physics are based upon the physics models and CZT tables within GATE, we assume an otherwise perfect detector performance (including Hit placement, energy resolution, and coincidence pairing) to focus on the physics at work. In other words, we assume the best-case scenario for such a technique as a demonstration.

This detector system is chosen for this study due to the high gamma interaction resolution it can achieve: 1×2.5 mm in x-y and sub-millimetre resolution in z. However, as we assume an ideal detector, making use of only the material cross section for the Monte Carlo simulation. Importantly, the elevated Compton scatter frequency of CZT benefits the

sensitivity of this potential technique. The panel spacing is adjustable and set to 20 cm as a target distance for high-resolution head and neck imaging studies.

Two categories of simulations are conducted: (1) with a pure positron emitter to demonstrate the difference in $\Delta\phi$ distributions based on the entanglement and polarization state of the annihilation gamma pair, and (2) with a dual positron and prompt gamma emitter to showcase the simple $\Delta\phi$ filtering approach. For both categories, a 30 μCi point source is centred in the system FOV with a 30 s collection period. For category (1), the source is an FDG-like positron emitter. Here, to emulate the different physics described by Eqs. 1–5, we conduct three separate simulations using the emlivermore, emlivermore_polar, and emlivermore + QE GATE physics lists. The emlivermore list uses no gamma polarization nor entanglement; the emlivermore_polar list accounts for gamma polarization but not entanglement; and the emlivermore + QE list accounts for both. For category (2), we use a Zr-89 ion source and the emlivermore + QE physics list. The GATE Hits output is recorded and processed with an in-house code for extracting the true DCSc events and their Compton and photoelectric absorption coordinates. These list-mode coordinates are subsequently used to compute their polar (θ) and azimuthal (ϕ) angles and their differential azimuthal angle ($\Delta\phi$).

RESULTS

Viewing Scattering Analytically

The three main gamma coincidence pair scenarios are when (1) there exists random polarization between the two gammas, (2) there exists orthogonal polarization but no entanglement between the two gammas, and (3) the two gammas are entangled and orthogonally polarized. A final possibility is where the two gammas are entangled but not orthogonally polarized, but achieving such requires that scattering events do not result in decoherence – a contested assumption and so it is not considered here.

We walk through a series of these scenarios in Fig. 3., visualising the (double, for some) differential cross sections normalized to represent occurrence. The dimensionality of the two-photon functions requires collapsing some terms to accommodate this visualisation. The first reduction is the simplification that $\theta_1 = \theta_2$ – this step is analogous to polar filtering, where a given DCSc will only be considered if the polar scattering angle is within some window (typically tens of degrees about 90°). Second, $\Delta\phi$ is occasionally considered as opposed to ϕ_1 and ϕ_2, individually, as is the case in Fig. 3C. and 3D.

Between the two single photon cases (no entanglement) in Fig. 3A. and 3B., we can see that the effect of polarization introduces moderate ϕ modulation. While the maximally occurring scatter is about $\theta = 0°$ for both, off-maxima occurrence is heightened for ϕ about ±90° with polarization. Shown in Fig. 3B. is but one possible linear polarization state; as the polarization direction changes, the bands about $\phi = \pm 90°$ shift left or right accordingly. Averaging across all these possibilities recaptures the non-polarized case illustrated in Fig. 3A.

When we consider entanglement in Figs. 3C. and 3D., moving from a ϕ-basis to a $\Delta\phi$-basis, we tenuously observe independence on $\Delta\theta$ in Fig. 3C. In the surface plot, some $\Delta\phi$ modulation about $\theta = \pm 60°$ appears, but it is weak. Taking the log of the z-axis helps distinguish this topology in Fig. 3D. This feature is better seen when viewing ϕ_1 *vs* ϕ_2 as opposed to θ *vs* $\Delta\phi$. Fig. 3E. shows the non-entangled but orthogonally polarized case, while Fig. 3F. shows when the same pair is entangled. The polarized case is maximized for $\Delta\phi = 0°, \pm 180°$, while the entangled case is maximized for $\Delta\phi = \pm 90°$. We can also note the difference in expected occurrence (z-axis) between these where the non-entangled case has ~10x the maxima of the entangled case (as compared to the respective minima) – i.e., the non-entangled case has better contrast. Of course, the frequency of non-entangled but orthogonally polarized photon pairs is uniform across all polarization states; and so, Fig. 3E. is the distribution for just one case of a false coincidence pair.

We narrow the scope from Fig. 3C. to the θ slice where the contrast with respect to $\Delta\phi$ is maximized – occurring at $\theta = 81.7°$ – in Fig. 4. (left). Here, we compare the enhancement ratio (the maximum-to-minimum ratio) across the three earlier scenarios. The entangled case exhibits the strongest $\Delta\phi$ modulation with a peak value of ~2.83; the orthogonally polarized case has a peak of ~1.63. There is no modulation for randomly polarized gamma pairs – for which orthogonal polarization is one such case.

$\Delta\phi$ Filtering Performance

We begin by adjusting the enhancement ratio (or relative occurrence) in Fig. 4. (left) to the likelihood in Fig. 4. (right) – we do so by setting their integrated densities to unity for 1° step size. This plot can be interpreted as the likelihood of a photon pair with the corresponding physics scattering with $\theta_1 = \theta_2 = 81.7°$ into each 1° $\Delta\phi$ bin. One may assume that direct $\Delta\phi$ filtering may be reasonable based on this plot – if we draw a window about $\Delta\phi = \pm 90°$, there would be a greater number of trues (entangled pairs) than random and scatter pairs (non-entangled with random polarization). However, this assumes equal true and false coincidence rates.

Using the true (0.372 fraction) and false (0.628 fraction) coincidence rate for our 2-Panel system from a simulated characterisation study (Fig. 6., 40 kBq/cm^3 in reference [11]), we scale these individual likelihoods to actual frequencies in Fig. 5. (left). We can now observe that the random and scatter frequency is always greater than the true frequency, regardless of $\Delta\phi$. While it is obvious that using a “keep” window about any $\Delta\phi$ angle would result in a False Positive rate > True Positive rate, we still display this in Fig. 5. (right), drawing a window about $\Delta\phi = 90°$. The density (or fraction) of true coincidences captured is always less than that of the false ones – this capture rate worsens with a wider window.

SIMULATION RESULTS

We extract the DCSc events for each of the simulations and plot them in Fig. 6. with an accepted polar scattering of $\theta \in \pm[70°, 90°]$. The varied physics scenarios plotted in Fig. 6. (left) closely match the expected distribution in Fig. 4A. – the notable difference in magnitude is primarily attributable to the non-zero θ window width required with the

data-based approach. It is important to note that the “emlivermore” case has no polarization whatsoever – however, this is practically equivalent to random polarization.

As the polarization between annihilation gammas and prompt gammas are independent, when paired, their expected count *vs* $\Delta\phi$ plot should be uniformly distributed. We make this observation in Fig. 6. (left). As before, the correctly paired set (annihilation gammas with each other) matches the analytical expectation (accounting for θ bin size). So, while $\Delta\phi$ modulation is much stronger for true pairs than annihilation-prompt pairs, based on our finding in Fig. 5., we should not expect direct filtering to be a successful discrimination technique.

DISCUSSION

The notion of using entanglement-based physics to distinguish true coincidences, randoms and scatters in PET is an exciting proposition. As shown in Fig. 4, there is information accessible to users to inform a classification algorithm of some variety. The orthogonal scattering of entangled photons (true coincidences) is theoretically 2.83 times greater than that for non-entangled photon pairs (randoms and scatters). When adjusting for likelihood (Fig. 4. (left)), this ratio effectively means that (in a perfect world) for every ~1.5 correctly classified true coincidence, 1 false pair will be incorrectly assigned true status. While orthogonally polarized photons also have an increased scatter rate for $\Delta\phi = \pm 90°$, this is less important for two reasons. Firstly, it is due to the smaller peak enhancement ratio. Second, and more notably, noise coincidences will have random relative polarization. For a population of random coincidences, the scatter frequency will be uniform in $\Delta\phi$ – an effective averaging over all polarization states nets the original Klein-Nishina case in Eq. 1. Thus, the enhancement ratio is generally a viable target for noise-reduction techniques.

When accounting for actual true and noise coincidence rates, however, this relationship substantially shifts in favour of noise. Any 1D thresholding technique based on $\Delta\phi$ will result in excessively poor true positive and false positive rates as captured by our filtering results. In fact, the accuracy of such a technique is dependent upon the relative noise and true rates. For equal rates, Fig. 4. (right) describes the expected curves (entangled – blue, and randomly polarized – green) one would use for thresholding. As the relative rates change, the curves would move up or down with respect to each other. In the case of our 2-Panel system, the noise rate exceeds the true rate at all possible thresholding levels. Further considerations for the non-collinearity of annihilation gammas must also be addressed. Deviations in the typically assumed back-to-back flight trajectory, while small, may result in significant errors in scattering vector extraction for scanners with large gantries. This potential source of error must be further explored.

The ability to incorporate this a priori scattering knowledge must be done in a more sophisticated fashion. Watts et al described an image-based method which requires a system characterisation study to estimate the relative noise and true signals in each reconstructed voxel [4]. Such a technique does not rely on event-by-event discrimination but instead the total image response to this physics. While simple $\Delta\phi$ filtering may not be feasible, there

may be more advanced classification techniques which enable interaction with list-mode data as opposed to image-based methods. We leave this as future work for consideration.

CONCLUSION

We have shown that the theoretical expectation of filtering DCSc coincidence data with a simple $\Delta\phi$ filter to discriminate between true coincidences *versus* random and scatter coincidences. The proclivity of true gamma pairs to scatter orthogonally to each other is a combination of their orthogonal polarization and entanglement. When looking at the polar scattering angle that maximizes the consequence of this effect ($\theta = 81.7°$), entangled gammas exhibit strong modulation with $\Delta\phi$, whereas non-entangled gammas with random polarization exhibited none. Accounting for the frequency of these events, however, demonstrates that a simple filter built around this physics is unfeasible. Whether discriminating true annihilation gamma coincidences from the prompt gamma signal or simple background reduction, a more sophisticated algorithm is needed to classify event-based data. We are conducting additional simulations to investigate the implications of detector characteristics on extracted $\Delta\phi$ distribution which are not considered in this work. While an ideal detector cannot distinguish trues from falses on an event-by-event basis, a real detector may still be able use $\Delta\phi$-based approaches for population-based filtering if sensitive enough to DCSc events and precise enough with their interaction location.

ACKNOWLEDGEMENTS

The authors acknowledge the support from the National Institute of Biomedical Imaging and Bioengineering of the National Institutes of Health under Award Number R01EB028091 and UG3EB034686.

REFERENCES

1. Bohm D, Aharonov Y. Discussion of experimental proof for the paradox of Einstein, Rosen, and Podolsky. Phys. Rev 1957;108(4):1070.
2. Pryce MHL, Ward JC. Angular correlation effects with annihilation radiation. Nature 1947;160(4065):435. [PubMed: 20265544]
3. Hartland SS, Pasternack S, Hornbostel J. Angular correlation of scattered annihilation radiation. Phys. Rev 1948;73(5):440.
4. Watts DP, Bordes J, Brown JR, Cherlin A, Newton R, Allison J, et al. Photon quantum entanglement in the MeV regime and its application in PET imaging. Nat. Commun 2021;12(1):2646. [PubMed: 33976168]
5. Alexander I, Abdurashitov D, Baranov A, Guber F, Morozov S, Musin S, et al. Testing entanglement of annihilation photons. Sci. Rep 2023;13(1):1–11. [PubMed: 36593249]
6. Sébastien J, Santin G, Strul D, Staelens S, Assié K, Autret D, et al. GATE: a simulation toolkit for PET and SPECT. Phys. Med. Biol 2004;49(19):4543. [PubMed: 15552416]
7. Agostinelli S, Allison J, Amako K, Apostolakis J, Araujo H, Arce P, et al. GEANT4 – a simulation toolkit. Nucl. Instrum. Methods Phys. Res. A: Accel. Spectrom. Detect. Assoc. Equip 2003;506(3):250–303.
8. Perkins ST, Cullen DE, Chen MH, Rathkopf J, Scofield J, Hubbell JH, et al. Tables and graphs of atomic subshell and relaxation data derived from the LLNL Evaluated Atomic Data Library (EADL), Z= 1−−100. No. UCRL-50400-Vol. 30. Lawrence Livermore National Lab. (LLNL), Livermore, CA (United States), 1991.

9. Enlow E, Diba M, Clayton J, Harris B, Abbaszadeh S. Impact of Flexible Circuit Bonding and System Integration on Energy Resolution of Cross-strip CZT Detectors. IEEE Trans. Radiat. Plasma Med. Sci 2023;7(6): 580–6. [PubMed: 38468608]

10. Yuli W, Herbst R, Abbaszadeh S. Development and characterization of modular readout design for two-panel head-and-neck dedicated PET system based on CZT detectors. IEEE Trans. Radiat. Plasma Med. Sci 2021;6(5):517–21. [PubMed: 37711549]

11. Mohan L, Yockey B, Abbaszadeh S. Design study of a dedicated head and neck cancer PET system. IEEE Trans. Radiat. Plasma Med. Sci 2020;4(4):489–97. [PubMed: 32632397]

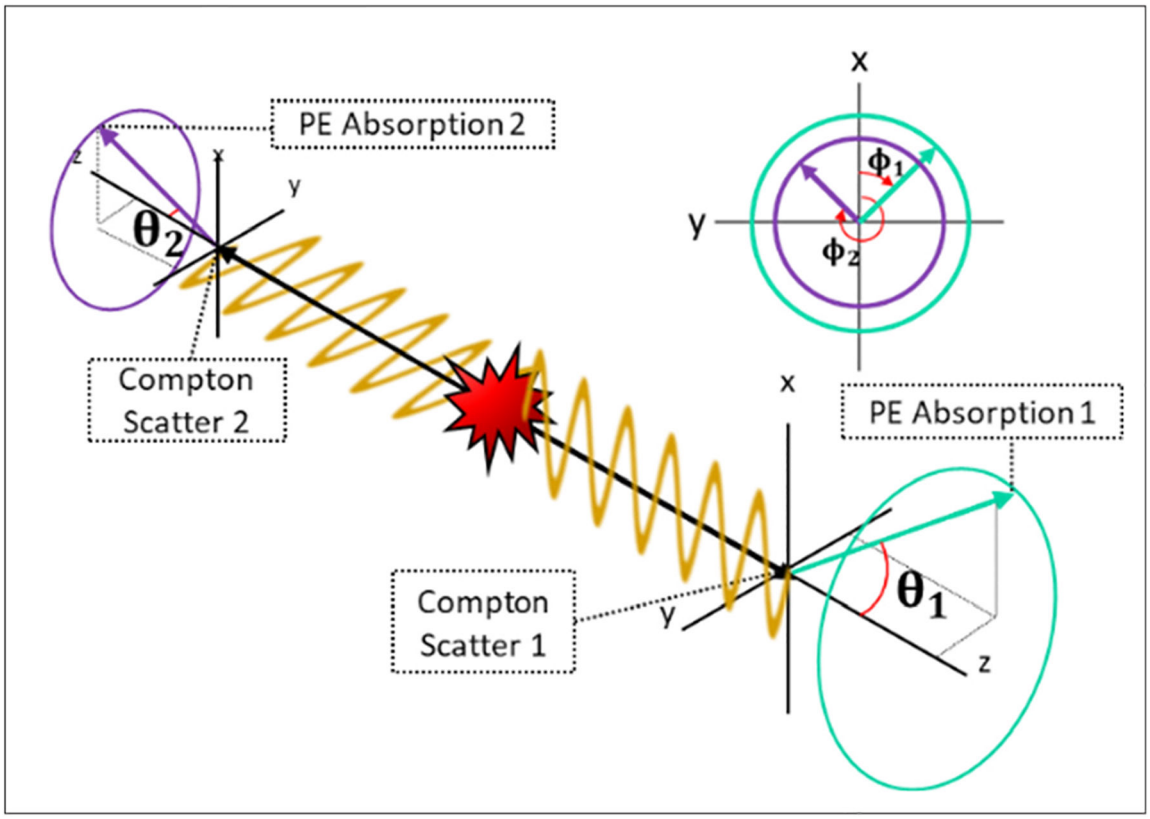

Fig. 1.

A diagram of a DCSc event where the orthogonal, linearly polarized photons each Compton scatter with a polar angle of θn and an azimuthal angle of ϕn and are subsequently absorbed.

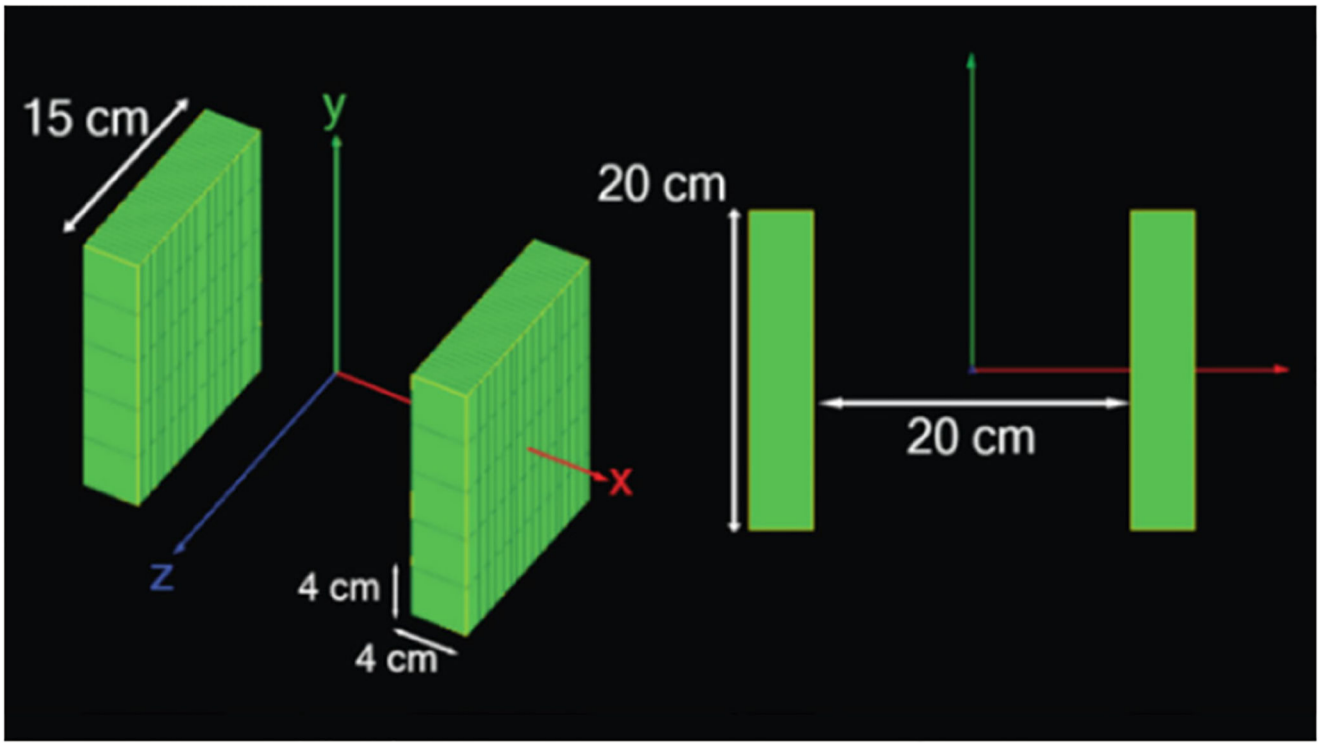

Fig. 2.
Depiction of the 2-Panel system defined in GATE.

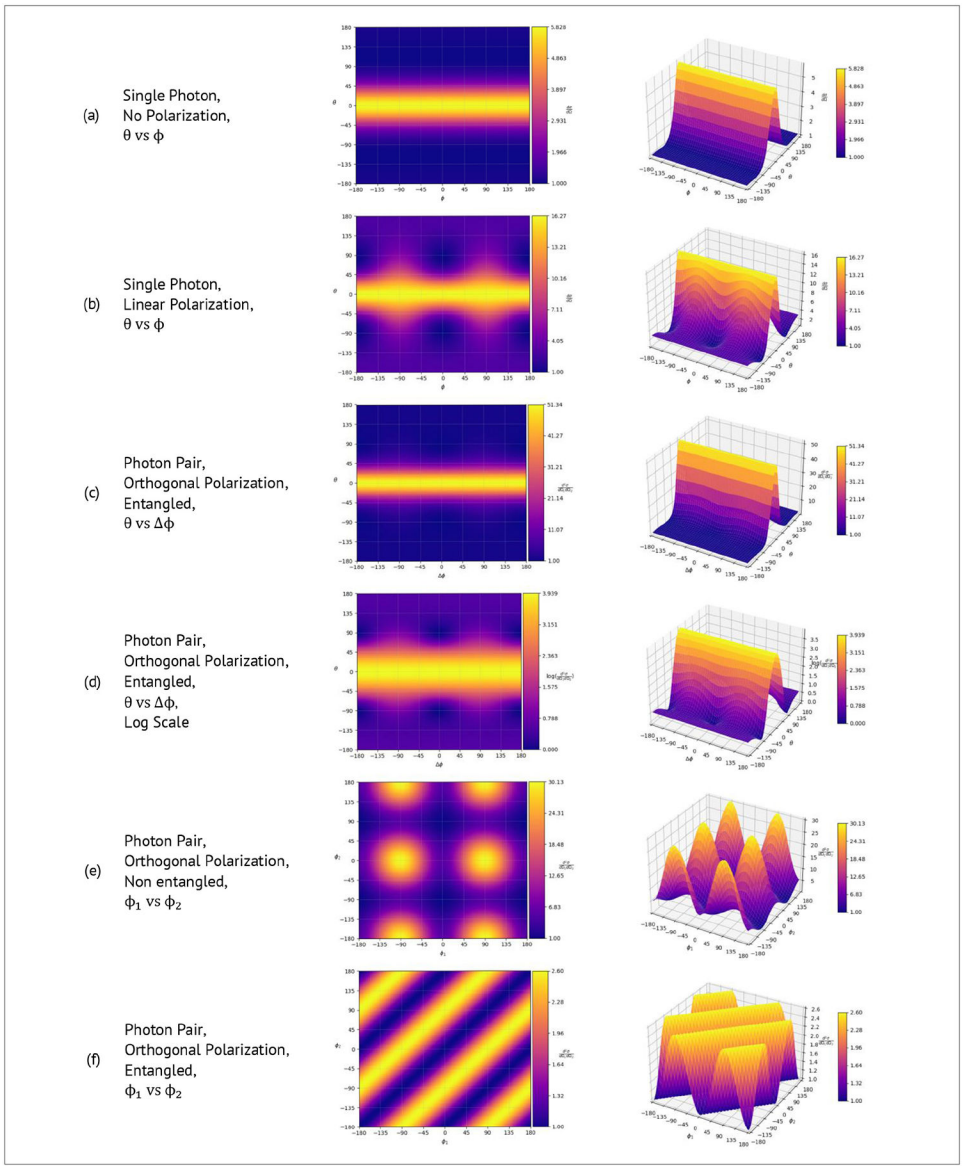

Fig. 3.

The single and double differential scattering cross sections standardized to the function's minimum for the various polarization and entanglement cases described above.

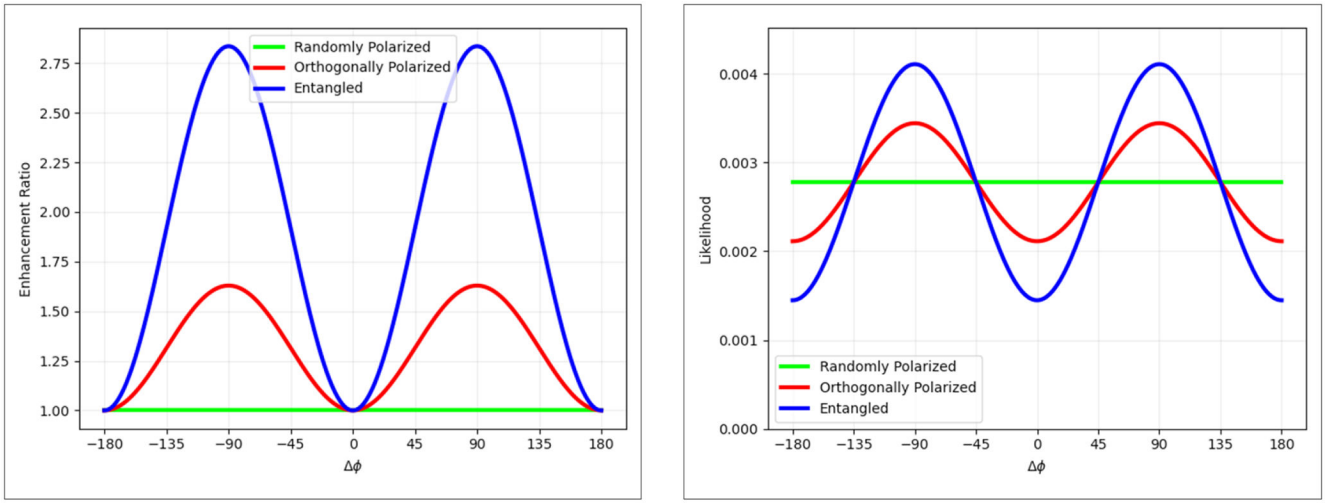

Fig. 4.

(left) The theoretical Enhancement Ratio (R) *vs* Δϕ for θ = 81.7° and with three gamma pair cases: (green) random, linear polarization, (red) orthogonal, linear polarization, and (blue) entnagled photons with orthogonal, linear polarization. (right) The likelihood of scattering in each 1° bin for the aformentioned polarization and entnaglement combinations.

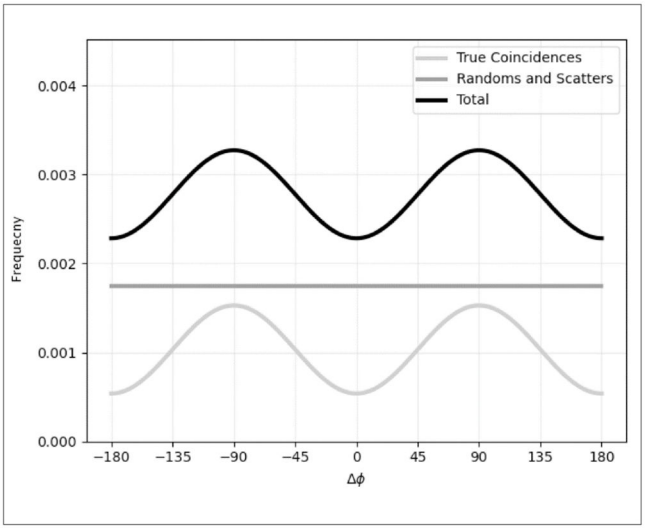

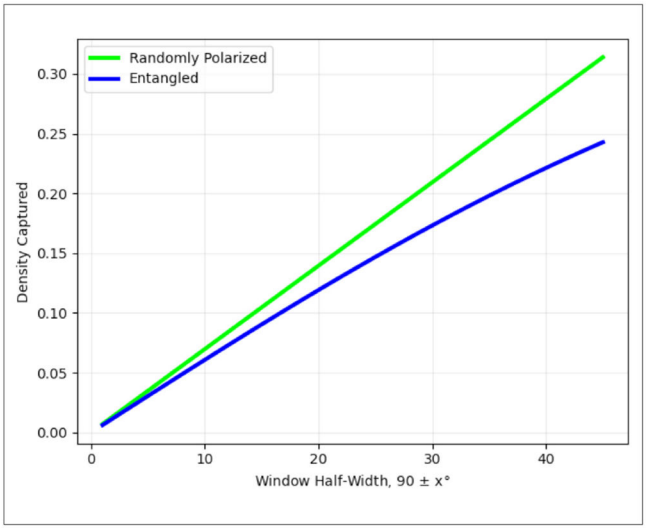

Fig. 5.

(left) The frequency of scattering into each Δϕ bin (1° bins) based on the likelihood in Fig. 4. (right) and the true and false coincidence fractions of 0.372 and 0.628, respectively. (right) The density captured of entangled photons pairs (true coincidences) and randomly polarized coincidenced (false coincidences) when drawing a window about the Δϕ = ±90° peaks in the left plot.

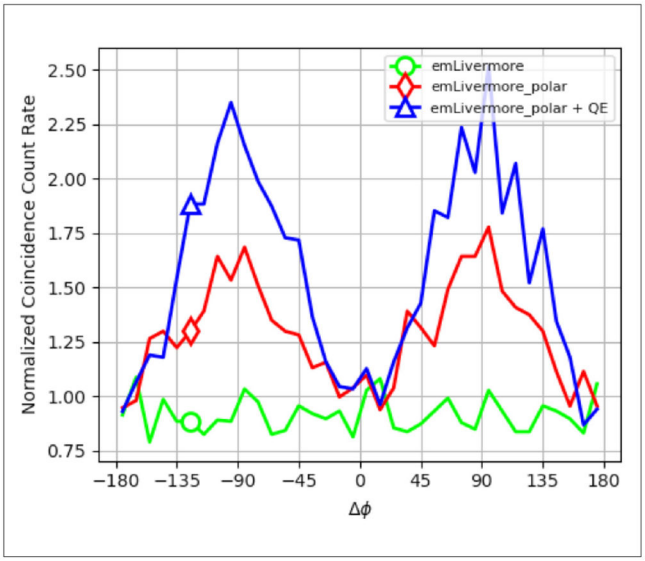

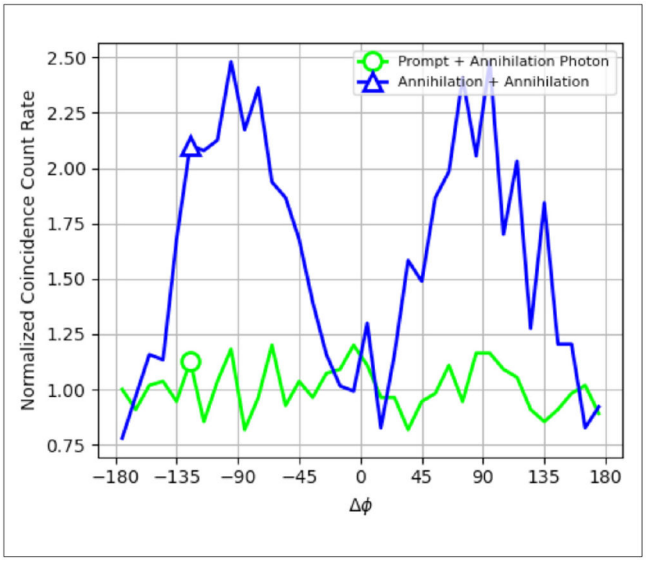

Fig. 6.

(left) The coincidence count rate normalized to the $\Delta\phi = 0°, \pm 180°$ bins for different GATE physics lists accounting for the polarization and entanglement states of: (green) random, linear polarization, (red) orthogonal, linear polarization, and (blue) entangled photons with orthogonal, linear polarization. (right) The coincidence count rate normalized to the $\Delta\phi = 0°, \pm 180°$ bins for: (green) prompt gammas incorrectly paired with annihilation photons, and (blue) annihilation photons correctly paired with eachother.